(Received 8 April 2026, Accepted 27 April 2026, Scheduled 17 May 2026)

A Miniaturized Low-Profile Wideband Filtering Antenna

Angen Guo[1], Zhonggen Wang[1], Wenyan Nie[2,*], and Han Lin[1]

[1] School of Electrical and Information Engineering, Anhui University of Science and Technology, Huainan 232001, China
[2] School of Mechanical and Electrical Engineering, Huainan Normal University, Huainan 232001, China

ABSTRACT: This paper presents a compact, low-profile, single-layer filtering antenna. The antenna features a simple structure comprising a dielectric substrate, two pairs of U-shaped defected ground structures, a symmetric dumbbell-shaped radiating patch, and a microstrip cross-feed line with asymmetric branches. The symmetric dumbbell-shaped patch and asymmetric branch feedline collaboratively excite additional high-frequency resonances, thereby broadening the impedance bandwidth. Furthermore, two pairs of U-shaped slots are etched into the bottom layer to introduce two radiation nulls on both sides of the passband, enhancing the frequency selectivity at the band edges and optimizing the antenna's radiation and filtering performance. To validate the proposed design, a prototype of the antenna was fabricated and measured. The simulated and measured results are in good agreement. The design achieves a wide impedance bandwidth of 48.6% from 3.7 to 6.18 GHz (centered at 5 GHz), a peak realized gain of 4.5 dBi, and a compact overall size of 35 mm × 29 mm × 0.8 mm. Moreover, the antenna structure is simple and is readily fabricated. Benefiting from its superior radiation performance and filtering characteristics, the proposed antenna is well-suited for wireless communication applications in the 5G Sub-6 GHz and WiFi-6E bands.

1. INTRODUCTION

In recent years, with the rapid advancement of wireless communication technologies, the requirements for radio frequency (RF) front-ends in terms of miniaturization, integration, and multifunctionality have been continuously rising [1]. In conventional RF front-ends, antennas and filters are designed as two separate key components, antennas are used for receiving and transmitting signals, while filters suppress unwanted interfering electromagnetic signals. These components are then cascaded directly to construct a complete RF front-end. Typically, a matching circuit is required between them to prevent impedance mismatch, which inevitably introduces additional insertion loss. Nowadays, integrating filters and antennas into a single unit — referred to as a filtering antenna — combines the filtering function of filters with the radiation characteristics of antennas. Such antennas can significantly reduce the size of RF front-ends and effectively improve circuit integration.

Currently, the design methods for filtering antennas can be categorized into three main technical approaches [2]. The first method involves cascading antennas and filters through transmission lines [3–5]. This approach uses connectors or impedance-matching networks to connect independently designed filters and antennas in series, forming a complete filtering antenna system. However, this cascaded design increases structural complexity and manufacturing costs. The second method employs the final resonator of a multi-resonator coupled bandpass filter as the radiating element [6–8], effectively overcoming many limitations of cascaded designs. The third method introduces special designs in the patch or feed structure to generate radiation nulls near the operating band [9–23]. This is achieved through various techniques introducing slots [9, 10, 12, 14], adding parasitic patches [11, 16, 18], using shorting vias [17, 19], employing defected ground structures (DGS) [13, 15, 20], and stacking patches [21, 22, 23] to achieve the desired filtering response. In most wideband filtering patch antenna designs, these techniques are often combined to simultaneously achieve wide bandwidth and high out-of-band suppression. However, the operating bandwidths of these reported antennas [9, 12, 13, 15] remain quite limited, and some designs of antennas [19, 21–23] are relatively complex. Therefore, developing a compact filtering antenna with a wide bandwidth is highly desirable.

In the sub-6 GHz band targeted in this work, planar microstrip-based filtering antennas are preferred for their inherent advantages in compactness, light weight, ease of integration with active circuits, and compatibility with mass-production PCB processes. The challenge lies in achieving wide bandwidth, sharp filtering selectivity, and low profile simultaneously on a single-layer microstrip substrate, as most existing designs resort to multi-layer stacking [18, 21, 22], shorting vias [17, 19], or additional lumped/distributed filtering circuits [3–5] to meet these requirements. Unlike prior works that rely on cascaded multi-layer structures, stacked patches, or lumped filtering circuits to achieve filtering performance, the novelty of this work lies in the synergistic integration of an asymmetric cross-feed line with a symmetric dumbbell-shaped patch and dual pairs of asymmetric U-shaped defected ground slots. This specific combination enables simultaneous wideband operation and a fully single-layer, low-profile realization — all without any additional filtering structures or shorting vias. Compared to other designs, the proposed antenna uses only a single-layer substrate and achieves a wider operating

* Corresponding author: Wenyan Nie (wynie5240@163.com).

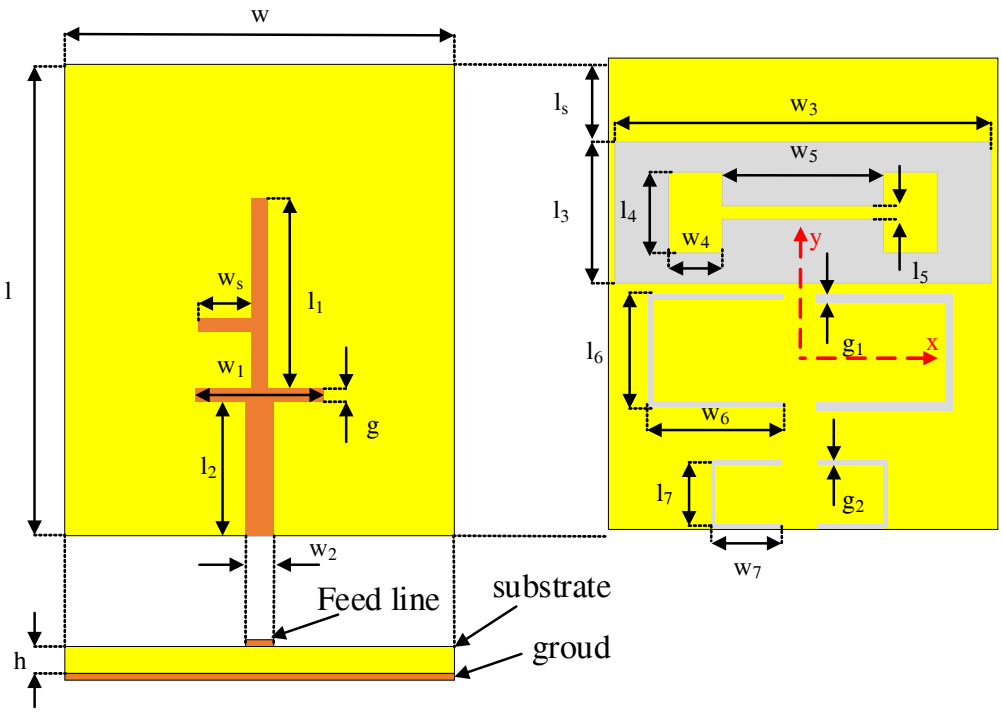

FIGURE 1. Geometry of the proposed antenna.

TABLE 1. Dimensions of the antenna (mm).

Parameter	l	l_1	l_2	l_3	l_4	l_5	l_6	l_7	l_s
Value	35	14.2	10	10.5	6	1	7	5	5.5
Parameter	w	w_1	w_2	w_3	w_4	w_5	w_6	w_7	w_s
Value	29	9.6	2.1	28	4	12	10.2	5	4
Parameter	h	g	g_1	g_2					
Value	0.8	1	0.6	0.3					

bandwidth. A prototype has been fabricated and measured. Simulated and measured results are presented and discussed.

2. FILTERING PATCH ANTENNA DESIGN

2.1. Antenna Configuration

The overall structure of the proposed filtering patch antenna is shown in Figure 1, with the detailed dimensions of key antenna components labeled. The antenna is designed on a single dielectric substrate and includes a defected ground layer with a dumbbell-shaped aperture etched in a rectangular area, along with two pairs of U-shaped slots of different sizes symmetric about the y-axis. The dielectric substrate is FR-4 with a relative permittivity (ε_r) of 4.4, a loss tangent ($\tan\delta$) of 0.02, and dimensions of 35 mm $\times$ 29 mm $\times$ 0.8 mm The top layer of the substrate features an asymmetric microstrip feed line: an additional branch is introduced on one side at three-fifths of the length of the cross-shaped feeder, forming an asymmetric microstrip feed structure. On the bottom layer, a dumbbell-shaped area is etched, and two pairs of U-shaped slots of different sizes symmetric about the y-axis are etched to generate two radiation nulls at low and high frequencies, respectively, thereby improving the out-of-band rejection performance of the filtering antenna. The detailed geometric dimensions are listed in Table 1.

2.2. Antenna Design Process

Figure 2 shows the complete design evolution of the antenna and explains the realization of the filtering performance step by step. Reference Antenna I (Ant. I) is a conventional rectangular wide-slot microstrip antenna, with a rectangular defected ground plane on the bottom layer and a cross-shaped microstrip feed line on the top layer. Reference Antenna II (Ant. II) is modified by adding a stub on one side of the cross-shaped microstrip feed line, and two pairs of U-shaped gaps symmetric about the y-axis are etched in the rectangular defected ground plane on the bottom layer. Reference Antenna III (Ant. III) has been improved based on the original design, rectangular defect ground planes in the bottom layer have been etched to form symmetrical dumbbell-shaped metal patches along the y-axis and two pairs of U-shaped slots. Based on Ant. II and Ant. III, the reference Antenna IV (Ant. IV) combines the stub and dumbbell-shaped structures. The proposed Antenna V (Ant. V) is further optimized by etching two pairs of U-shaped slots of different sizes into the bottom layer. Figure 3 compares the

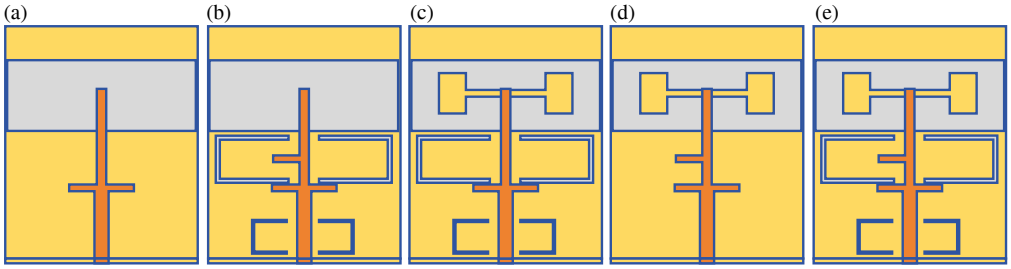

FIGURE 2. Evolution of the proposed filtering antenna. (a) Reference antenna I, (b) Reference antenna II, (c) Reference antenna III, (d) Reference antenna IV, (e) Proposed antenna V.

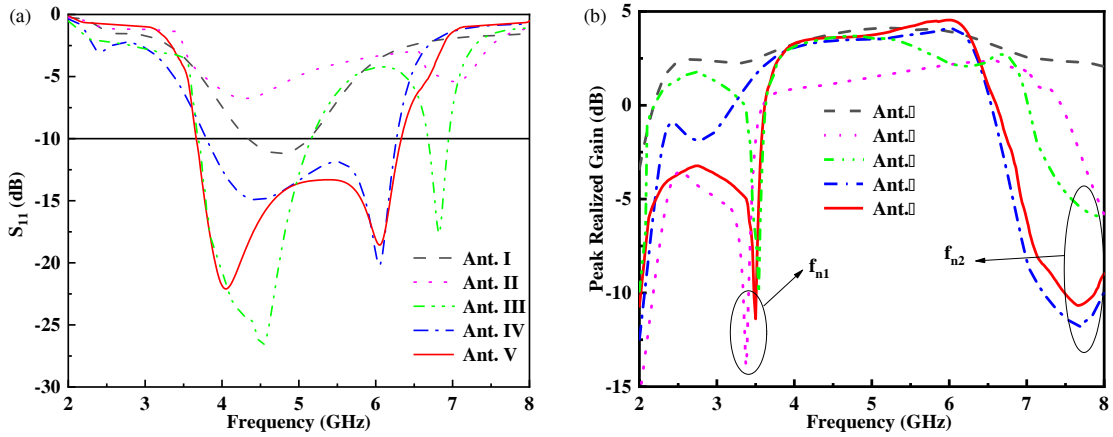

FIGURE 3. Simulated S_{11} and realized gains of the reference antennas and proposed antenna. (a) Simulated S_{11} curves, (b) Simulated realized gain curves.

simulated S_{11} parameters and realized gains of the reference antennas and the proposed antenna. As shown in Figure 3(a), Ant. I has a single resonant peak at 4.8 GHz, with an impedance bandwidth of approximately 16.7% (4.4–5.2 GHz) based on the -10 dB return loss criterion. Figure 3(b) shows that Ant. I has a peak gain of 4 dBi but exhibits poor out-of-band suppression and insufficient filtering performance. Therefore, at the bottom layer of Ant. I, two pairs of U-shaped slots are etched, and an asymmetric branch was added to the cross-shaped microstrip feedline to obtain Ant. II, thereby generating a radiation null at 3.4 GHz. At the same time, the off-band radiation intensity at high frequencies significantly decreased. As shown in Figure 3(b), this design produced a low-frequency radiation null f_{n1}.

The bandwidth of Ant. I is insufficient, and its impedance bandwidth is only 16.7%. Therefore, at the bottom layer of Ant. I, a dumbbell-shaped metal patch and two pairs of U-shaped slots are etched to obtain Ant. III, which generates an additional resonant peak at 6 GHz. The newly added resonance point forms a dual resonance with the existing 4.8 GHz resonance point of Ant. I, and their frequency bands work in concert, successfully widening the operating bandwidth. This creates a high-frequency radiation null f_{n2}, as shown in Figure 3(b).

Ant. IV, which combines the shape of a dumbbell and short branches, achieves basic filtering performance initially. By achieving an organic coordination between the two resonant points, the S_{11} value within the passband is significantly reduced, reaching an industrial effective level, but its out-of-band rejection performance at low frequencies remains insufficient.

Ant. V is an integrated optimization solution, aiming to coordinate and integrate the filtering performance present in the aforementioned design schemes. Ant. I exhibited insufficient bandwidth and poor out-of-band rejection, thus a dumbbell-shaped metal patch was introduced into the rectangular defected ground plane to add an additional resonant peak, thereby effectively broadening the impedance bandwidth. Adding an asymmetric stub successfully introduced a radiation null at high frequencies, thereby improving out-of-band rejection. However, the low-frequency radiation null performance remained to be improved. To solve this problem, two pairs of U-shaped slots need to be reintegrated. The introduction of the U-shaped slots significantly improved the impedance matching at the low-frequency resonant point. The dimensions of the U-shaped slots for the two radiation nulls can be calculated as follows:

$$L_h = 2 \times (l_6 + 2 \times w_6) \tag{1}$$

$$f_h = \frac{c}{L_h \times \sqrt{(\varepsilon_r + 1)/2}} \tag{2}$$

$$L_l = 2 \times (l_7 + 2 \times w_7) \tag{3}$$

$$f_l = \frac{c}{L_l \times \sqrt{(\varepsilon_r + 1)/2}} \tag{4}$$

where L_h represents the total length of the two large U-shaped slots, and L_l represents the total length of the two small U-

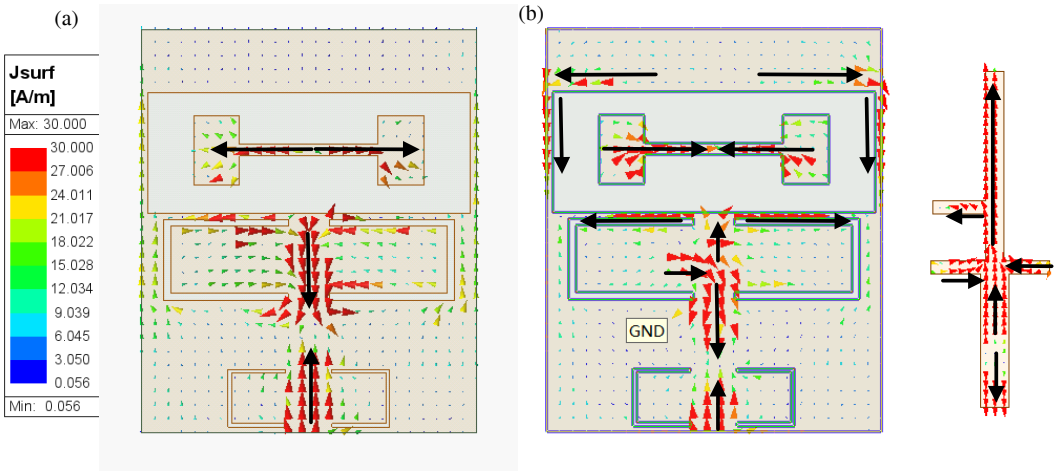

FIGURE 4. Current distribution of the proposed antenna at low and high frequencies.

shaped slots. Meanwhile, f_h is the frequency of the high-frequency radiation null, and f_l is the frequency of the low-frequency radiation null.

As shown in Figure 3(a), Ant. V exhibited a deeper resonance at 4 GHz. Based on the -10 dB return loss criterion, the antenna achieved an impedance bandwidth of approximately 48.6%, covering the frequency range from 3.7 GHz to 6.18 GHz. As shown in Figure 3(b), the frequency selectivity at the low-frequency band edge was significantly enhanced, and the gain response within the passband was flatter. The antenna achieved a peak realized gain of approximately 4.5 dBi and maintained a stable gain response over the entire passband. A radiation null was formed at 3.55 GHz in the lower stopband, with an out-of-band suppression level of more than 10 dB, which significantly improved the frequency selectivity of the lower stopband. In addition, another radiation null was formed at 7.67 GHz in the upper stopband, achieving a high out-of-band suppression level. The proposed antenna thus exhibited excellent filtering performance overall.

2.3. Operating Principle

To analyze the filtering performance of the proposed antenna, it is necessary to clarify the generation mechanism of the radiation nulls. Common methods for generating radiation nulls include adding parasitic elements, metal vias, and defected ground structures, as well as etching slots. Considering that the proposed antenna is designed for miniaturization and low profile, the available space for additional elements is limited; therefore, a defected ground structure and simple parasitic stubs are adopted. Two pairs of U-shaped slots are used to generate the radiation nulls for the low-frequency and high-frequency bands. Meanwhile, a parasitic shorting stub is employed to effectively adjust the high-frequency radiation null. The combined effect significantly enhances the out-of-band suppression performance of the antenna. Figure 4 presents the surface current distribution of the antenna at the low-frequency and high-frequency radiation nulls. The left part of Figure 4 shows the surface current distribution at the low-frequency radiation null f_{n1}. The surface current is mainly concentrated around the cross-shaped microstrip feed line, the two pairs of U-shaped slots, and the dumbbell-shaped patch. It can be clearly seen that the surface currents near the U-shaped slots and dumbbell-shaped patch have the same magnitude but opposite directions, flowing through the corresponding slots and forming a current distribution symmetric about the y-axis. Similarly, the surface currents on the cross-shaped microstrip feed line flow in three segments with equal intensity but opposite directions. Due to the electromagnetic coupling between the radiating patch and the bottom layer, these opposite currents induce destructive interference, which suppresses the antenna radiation. The etching of U-shaped slots alters the current distribution path of the bottom layer, forming a closed current loop around the slot, which runs opposite to the current direction of the feed line and the dumbbell-shaped patch. As a radiating unit, the hollowed-out structure of the dumbbell-shaped patch further enhances the current coupling between the bottom layer and the radiating patch, intensifying the phase cancellation effect, ultimately forming a radiation null. Therefore, the low-frequency radiation null f_{n1} is formed at 3.55 GHz (simulated value). The right part of Figure 4 shows the surface current distribution at the high-frequency radiation null f_{n2}. The surface current is mainly concentrated in the large U-shaped slot and the microstrip feed line. These surface currents have the same amplitude but opposite directions and are distributed symmetrically in the large U-shaped slot and the microstrip feed line. On the feed line, the asymmetric branches work in coordination to control the high-frequency radiation null to remain outside the passband. As a result, the radiation fields cancel each other out, leading to the formation of the high-frequency radiation null f_{n2} at 7.67 GHz (simulated value). Obviously, the formation of f_{n2} is a combined effect of the U-shaped slots and asymmetric microstrip feed line. These results verify that the dumbbell-shaped metal patch broadens the effective operating band, while the two pairs of U-shaped slots and the asymmetric microstrip feed line jointly expand the impedance bandwidth and improve the radiation performance of the antenna.

This dumbbell-shaped structure plays a crucial role in broadband operation, and its function goes beyond merely increas-

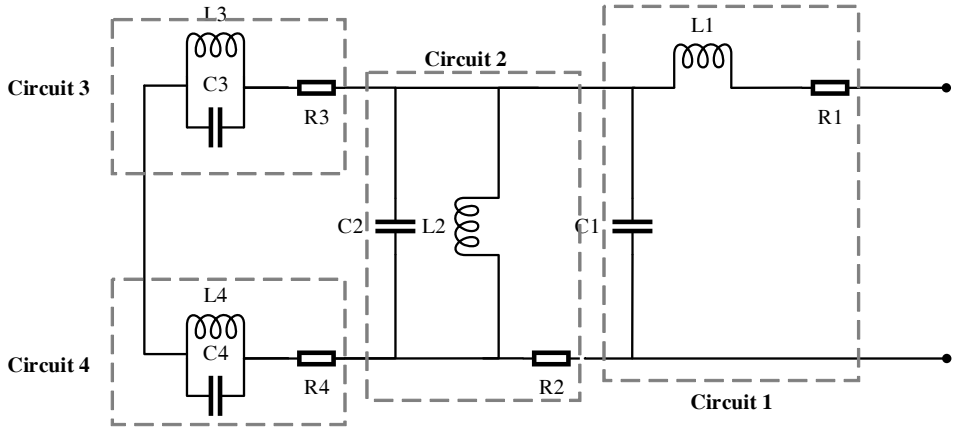

FIGURE 5. The equivalent circuit of the proposed filtering antenna.

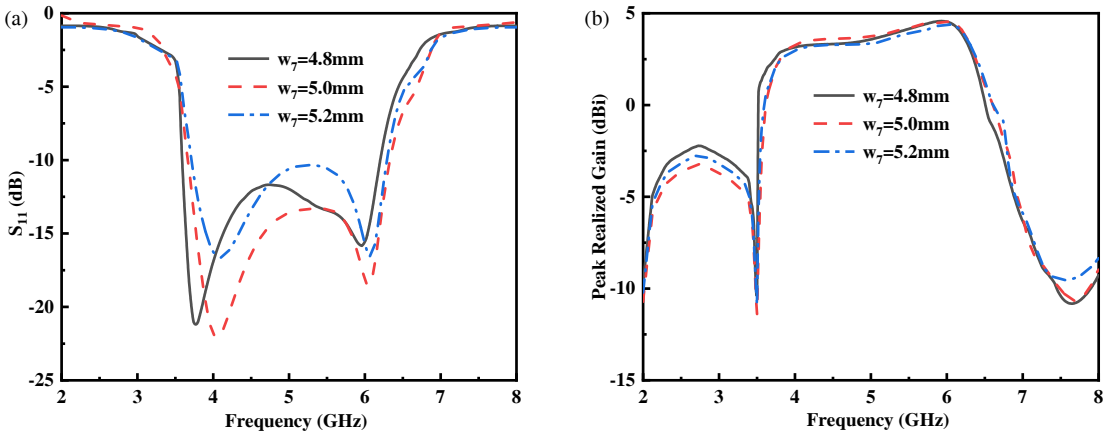

FIGURE 6. Simulated reflection coefficient and realized gain for different w_7 values.

ing the second resonance. By analyzing the current distribution shown in Figure 4, it can be observed that strong currents are concentrated at the edges of the dumbbell-shaped patch at both low and high frequencies. At the same time, we analyze the functions of the dumbbell-shaped structure, and the radiation nulls and resonance characteristics shown in Figure 3 indicate that the dumbbell-shaped structure not only acts as a radiation element but also serves as a coupling structure, significantly altering the effective current path on the grounding plane. Specifically, the hollow central area of the dumbbell-shaped patch introduces additional capacitive loading effects, combined with the linear U-shaped slot, forming a coupled resonator topology structure. This coupling mechanism enables the excitation of an additional higher-order resonant mode at approximately 6 GHz, which combines with the basic resonant mode of the rectangular aperture to form a wide continuous passband. Therefore, as a radiation patch, the dumbbell-shaped structure expands the effective aperture, and simultaneously, as a coupling element and impedance matching element, it changes the current distribution path to form a radiation null outside the high-frequency band. Figure 5 presents the proposed equivalent circuit of the antenna: Circuit 1 is composed of an asymmetric stub-fed line, while Circuit 2 is made up of a hollow dumbbell shape. Circuits 3 and 4 are respectively composed of two pairs of U-shaped slots. The dumbbell-shaped structure in this antenna plays a crucial role in widening the bandwidth by forming new in-band resonant points. Capacitors C3 and C4 represent the coupling capacitance between the U-shaped slots and the ground plane, and they are of great significance in optimizing the filter response to enhance its performance.

2.4. Parametric Study

To further investigate the radiation null characteristics of the antenna, specific structural parameters were analyzed, as shown in Figures 6, 7, and 8. The results show that by adjusting the key dimensions of the U-shaped slots, the radiation nulls of the proposed filtering patch antenna can be effectively tuned. Figures 6 and 7 show the effects of parameter variations on the reflection coefficient and realized gain, confirming that the positions of radiation nulls can be adjusted through structural optimization. Figure 6(a) presents the simulated reflection coefficient for different values of the U-shaped arm length w_7, and Figure 6(b) shows the corresponding realized gain curves. Figure 7 presents the simulated reflection coefficient and realized gain for different values of the short branch length w_s. Figure 8 shows the simulated reflection coefficients and actual gains under different values of the dumbbell-shaped gap length

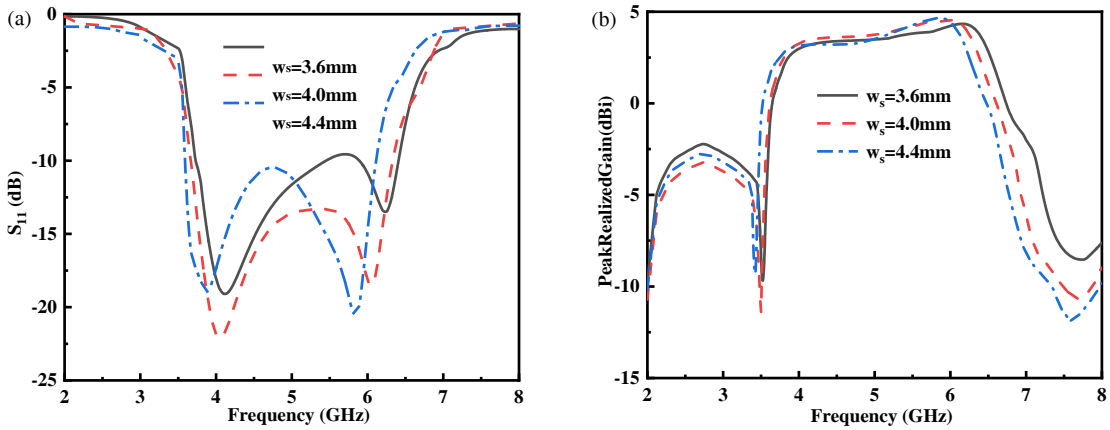

FIGURE 7. Simulated reflection coefficient and realized gain for different w_s values.

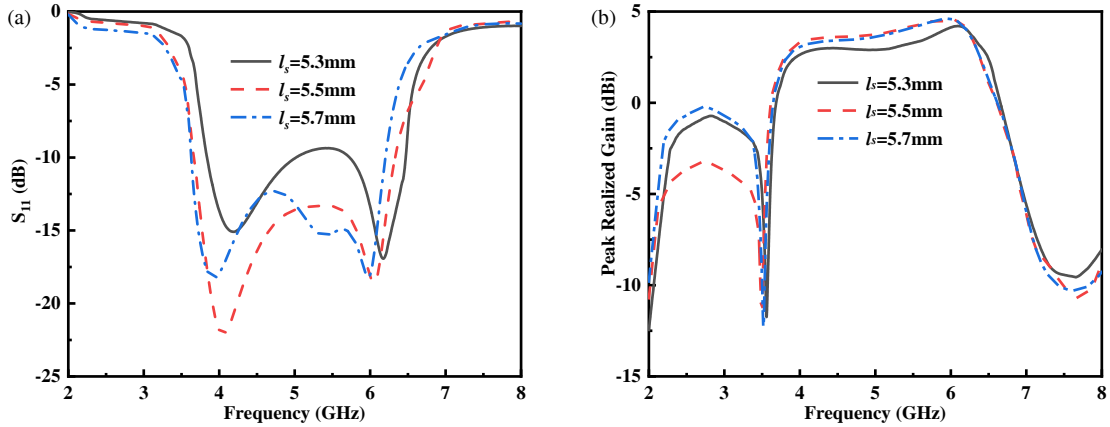

FIGURE 8. Simulated reflection coefficient and realized gain for differentl_s values.

l_s. When w_7 increases from 4.8 mm to 5.2 mm, the radiation null of the low-frequency resonance shifts towards a lower frequency range. In contrast, the high-frequency radiation null remains largely unaffected. Figure 6(b) shows that the change in w_7 has an insignificant effect on the high-frequency radiation null, which proves that adjusting w_7 can independently control the low-frequency radiation null. When the width of w_s increases from 3.6 mm to 4.4 mm, the high-frequency radiation null shifts towards a lower frequency direction, but the low-frequency radiation null remains stable. Figure 7(b) shows that the change in w_s has a negligible effect on the low-frequency radiation null, which proves that the high-frequency radiation null can be independently controlled by adjusting w_s. Although the changes in these two key parameters would simultaneously affect the in-band resonance, the effective frequency range of the antenna S_{11} remained largely unchanged. Therefore, it can be concluded that the low-frequency and high-frequency radiation nulls are mainly independently controlled by the U-shaped slot structure and shorting stubs, respectively. As can be seen from Figure 8(a), the position of the dumbbell-shaped defect structure has a regulating effect on the in-band resonance. When the value of l_s increases from 5.3 mm to 5.7 mm, both of the two resonant points within the band shift to a lower frequency range, and the effective frequency band also shifts; in contrast, Figure 8(b) indicates that the change in l_s has basically no effect on the radiation zero point of the antenna, which proves that by adjusting l_s, the working frequency band of the antenna can be adjusted. By adjusting these parameters, the radiation null positions of the antenna can be effectively tuned. When $w_7 = 5.0$ mm, $w_s = 4.0$ mm and $l_s = 5.5$ mm, the antenna achieves a radiation null suppression depth of over 10 dB at both 3.55 GHz and 7.67 GHz, with a -10 dB impedance bandwidth of 48.6% and optimal gain flatness in the passband (fluctuation below 0.5 dBi). Therefore, parameters are selected as the optimal values.

3. MEASUREMENT AND COMPARISON

3.1. Antenna Model Measurement

The proposed filtering antenna was designed and simulated using the High Frequency Structure Simulator (HFSS) electromagnetic simulation software. To verify the theoretical model, a prototype of the antenna was fabricated, and an SMA coaxial connector was soldered to the end of the microstrip feed line. Figure 9(a) shows the fabricated prototype of the compact broadband filtering antenna. The S-parameters and radiation characteristics of the prototype were measured using an AV3629D vector network analyzer in a microwave ane-

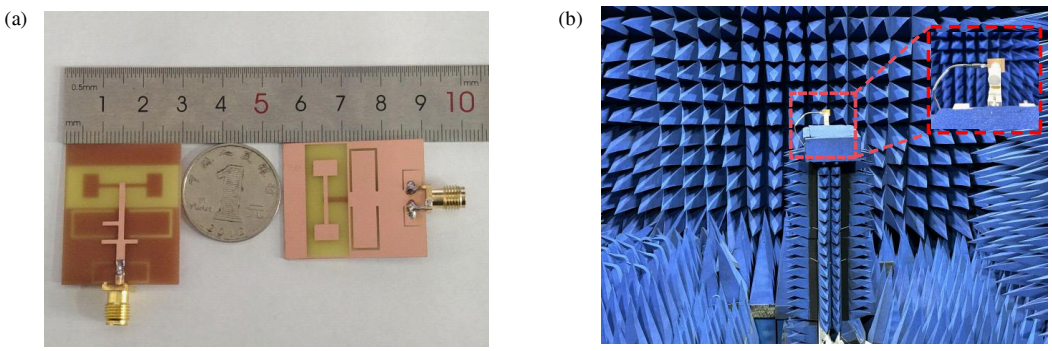

FIGURE 9. Photographs of the fabricated antenna and measurement environment.

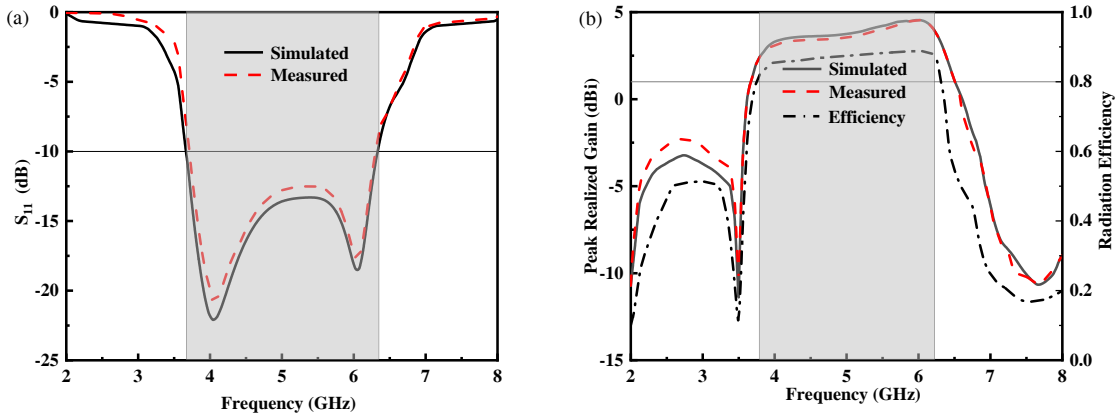

FIGURE 10. Simulated and measured S_{11}, realized gains, and radiation efficiencies of the filtering antenna. (a) S_{11}. (b) realized gain and radiation efficiency.

choic chamber, as shown in Figure 9(b). Figure 10 compares the simulated and measured S-parameters, realized gains, and radiation efficiencies of the antenna, and the results are in good agreement. The measured results of Figure 10(a) show a -10 dB impedance bandwidth of 48.6% (3.7–6.18 GHz), with two distinct resonant peaks at low and high frequencies. Figure 10(b) shows that the gain curve is relatively flat within the passband, with a simulated peak realized gain of 4.5 dBi and a measured value of 4.3 dBi; the gain drops sharply outside the passband. The realized gain within the 3.7–6.18 GHz passband exhibits a measured variation of less than 1.8 dB (from 2.6 to 4.4 dBi), with a peak-to-average gain ratio of approximately 1.5 dB. Over the central 80% of the band (4.0–5.8 GHz), the gain flatness is further improved to within ± 0.5 dB, demonstrating stable radiation performance suitable for wideband communication systems. This flat gain response is attributed to the well-merged dual-resonance modes enabled by the dumbbell-shaped patch, which mitigate the gain dip typically observed between widely separated resonant frequencies. The measured peak realized gain is 4.3 dBi (simulated 4.5 dBi). The good agreement between the simulated and measured results verifies the excellent filtering performance of the antenna. The consistency between the two is attributed to the simplicity of the proposed antenna structure, the absence of additional filtering structures, and the relatively low insertion loss. The deviations mainly result from the minor errors in processing and measurement. In addition, radiation nulls are observed at 3.55 GHz and 7.67 GHz on both sides of the passband. Within the 3.7–6.18 GHz passband, the measured radiation efficiency of the antenna ranges from 80% to 88%, with an average of 84%, indicating that the antenna exhibits low-loss characteristics. Two nulls are clearly visible in the efficiency curve, further demonstrating the antenna's high efficiency, low loss, and high frequency selectivity. Figure 11 presents the simulated and measured E-plane (xz-plane) and H-plane (yz-plane) radiation patterns of the antenna at the two resonant frequencies. Figure 12 shows the three-dimensional radiation pattern of the antenna at different frequencies. Co-polarization is dominant in the main radiation direction, with a cross-polarization suppression level of more than 20 dB, which indicates good polarization purity and verifies the excellent radiation performance of the antenna. The minor deviations between simulation and measurement mainly originate from three aspects: dimensional tolerance in FR-4 substrate etching (± 0.1 mm), impedance discontinuity at the solder joint between SMA coaxial connector and microstrip feed line, and systematic error in microwave anechoic chamber measurement (± 0.2 dBi).

3.2. Antenna Performance Comparison

To further demonstrate the advantages of the proposed filtering antenna, Table 2 compares it with previously reported fil-

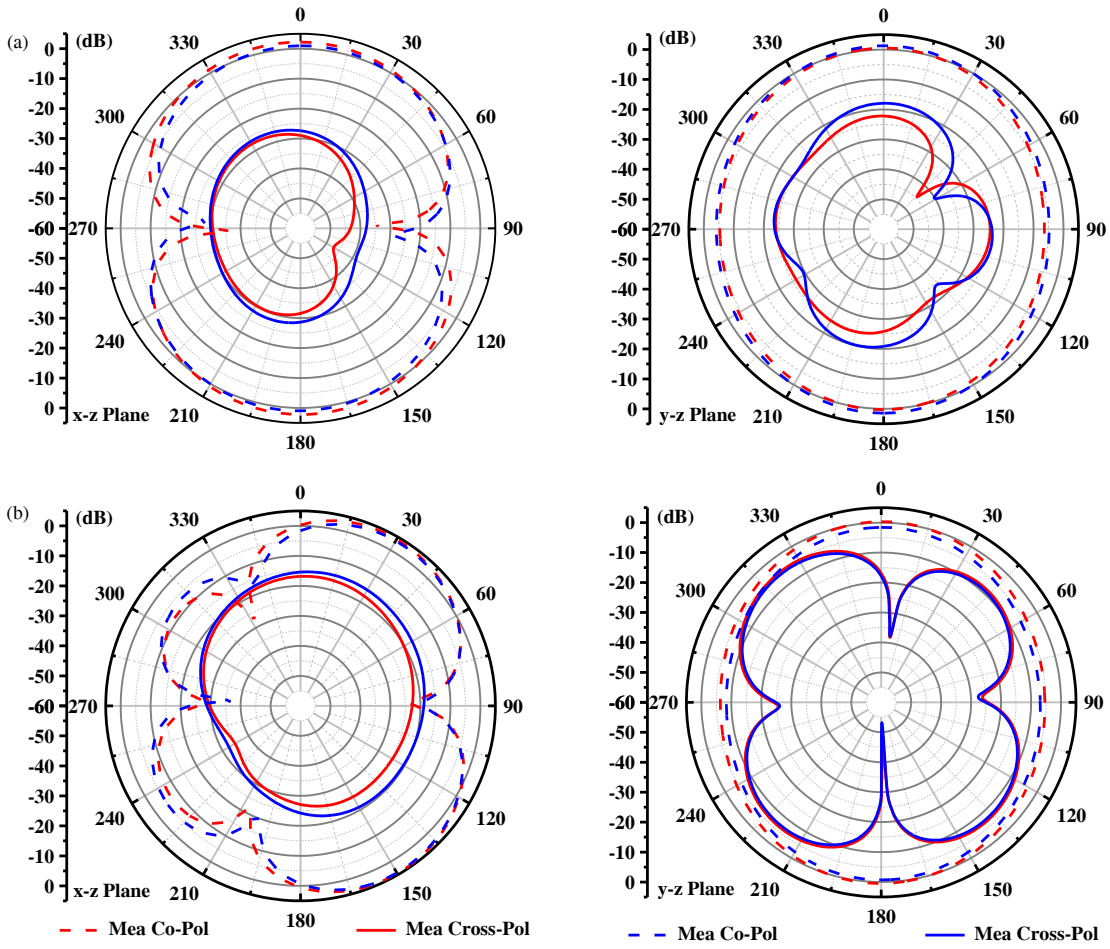

FIGURE 11. Simulated and measured radiation patterns of the filtering antenna in the xz and yz planes at different frequencies. (a) 4 GHz. (b) 6 GHz.

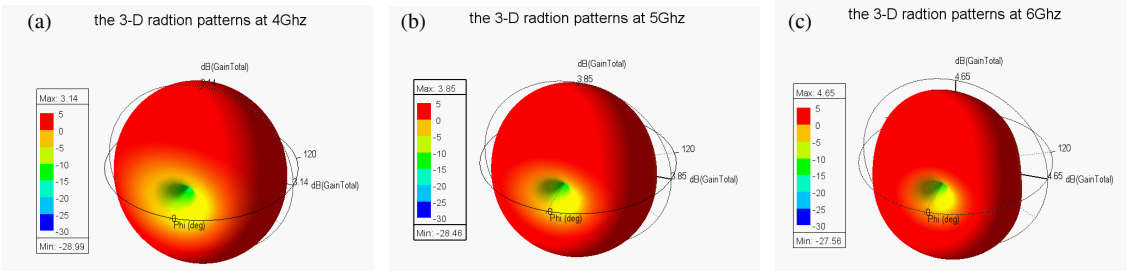

FIGURE 12. Three-dimensional radiation patterns of the filtered antenna at different frequencies. (a) 4 GHz. (b) 5 GHz. (c) 6 GHz.

TABLE 2. Performance comparison of filtering antennas. λ_0 is the free-space wavelength at the center frequency f_0.

Article	Profile (λ_0)	f_0 (GHz)	Size (λ_0^2)	BW (%)	Efficiency (%)	Gain (dBi)	Extra filtering structure
[9]	0.050	2.48	0.71×0.37	17.7	~ 92.1	8.1	Yes
[11]	0.007	2.05	0.48×0.34	33.8	NG	4.1	Yes
[13]	0.061	11.8	0.48×0.47	11.84	~ 82.3	5	No
[14]	0.090	5	0.4×0.4	21.5	~ 93	4.8	Yes
[15]	0.015	5.6	0.65×0.54	33.2	~ 86	4.92	No
[16]	0.050	2.49	0.58×0.38	16.1	~ 97	9.6	Yes
[23]	0.009	4	0.41×0.34	66.5	~ 92	4.25	No
This work	0.013	5	0.58×0.48	48.6	~ 84	4.5	No

tering antennas in the literature. As seen in the table, compared with [9, 15, 16], the proposed design features a simple structure, low profile, and relatively small footprint, meeting miniaturization requirements. Compared with filtering antennas without additional filtering structures [13, 15], the proposed antenna achieves a wider impedance bandwidth of 48.6%. Even compared with antennas having additional filtering structures [9, 11, 14, 16], its size and impedance bandwidth still show significant advantages. The proposed antenna exhibits a lower gain compared to the antennas presented in [9, 15, 16], but the gain is slightly higher than that of [11, 14, 23], and it is within the average range for filtering antennas. The primary advantage of the former antennas lies in their high gain. The measured gain (4.5 dBi) and the average efficiency compared to the simulation is 84%, which was mainly a compromise made for high bandwidth and miniaturized structure, as well as the inherent loss of the FR-4 substrate and the radiation limitations brought about by its low-profile design. It is worth noting that for the intended application scenarios — 5G Sub-6 GHz and WiFi-6E terminal devices — the achieved gain of 4.3 dBi (measured) is adequate, and the overall advantages in bandwidth, miniaturization, and single-layer, low-cost fabrication outweigh the moderate gain performance. Future improvements can be achieved by replacing the substrate with a low-loss alternative (e.g., Rogers RO4350). However, the main advantages of this antenna are its low profile and wide bandwidth. While achieving these advantages, the frequency selectivity of the proposed antenna reaches the average level of previously published filtering antennas. The performance comparison shows that the proposed antenna achieves a balanced trade-off among low profile, compact size, impedance bandwidth, efficiency, and gain.

4. CONCLUSION

This study has proposed and experimentally validated a low-profile filtering antenna that combines wide bandwidth with compact size. The proposed "dumbbell-shaped patch + dual U-shaped defected ground" integrated design approach provides a novel solution for single-substrate wideband filtering antenna development. The antenna achieves a balance between compact size (35 mm $\times$ 29 mm $\times$ 0.8 mm) and wide bandwidth without incorporating additional filtering structures. After fabricating and measuring the antenna prototype, the final design demonstrates excellent performance characteristics, including a wide operating bandwidth of 48.6% (3.7–6.18 GHz) and a peak realized gain of 4.5 dBi, making it directly applicable to the 5G Sub-6 GHz and WiFi-6E bands for terminal devices.

ACKNOWLEDGEMENT

This work was supported in part by the Natural Science Research Project of Anhui Educational Committee under Grant No. 2025AHGXZK31006, in part by the Research Foundation of Jiangsu Engineering Research Center for Bionics Control Technology and Equipment under No. FSKZ202503, in part by the Anhui International Joint Research Center for Ancient Architecture Intellisencing and Multi-Dimensional Modeling under No. GJZZX2025KF03.

REFERENCES

[1] Gui, H., Z. Wang, W. Nie, M. Yang, and M. Wang, "Design of a compact wideband filtering antenna with high frequency selectivity," *Progress In Electromagnetics Research M*, Vol. 131, 27–35, 2025.

[2] Kong, Y.-D., X.-C. Zhang, and Q.-X. Chu, "A wideband filtering antenna for wearable applications with high suppression level," *AEU — International Journal of Electronics and Communications*, Vol. 205, 156167, Feb. 2026.

[3] Zhang, Y.-M., S. Zhang, Q.-C. Ye, and G. F. Pedersen, "Cosynthesis of a filtering antenna with harmonic suppression," *IEEE Antennas and Wireless Propagation Letters*, Vol. 19, No. 10, 1729–1733, Oct. 2020.

[4] Sahu, B., S. Singh, M. K. Meshram, and S. P. Singh, "Integrated design of filtering antenna with high selectivity and improved performance for l-band applications," *AEU — International Journal of Electronics and Communications*, Vol. 97, 185–194, Dec. 2018.

[5] Lin, J.-Y., S.-W. Wong, L. Zhu, Y. Yang, X. Zhu, Z.-M. Xie, and Y. He, "A dual-functional triple-mode cavity resonator with the integration of filters and antennas," *IEEE Transactions on Antennas and Propagation*, Vol. 66, No. 5, 2589–2593, May 2018.

[6] Wu, Z., A. Zhang, J. Chen, X. Lu, and J. Li, "Co-design of low profile single-fed circularly polarized filtering antenna with high out-of-band rejection," *AEU — International Journal of Electronics and Communications*, Vol. 102, 99–104, Apr. 2019.

[7] Hong, W., Z.-J. Guo, and Z.-C. Hao, "Seamless integration technology for filtenna toward 5g/6g wireless communications," *IEEE Open Journal of Antennas and Propagation*, Vol. 5, No. 1, 18–36, Feb. 2024.

[8] Chen, F.-C., H.-T. Hu, R.-S. Li, Q.-X. Chu, and M. J. Lancaster, "Design of filtering microstrip antenna array with reduced sidelobe level," *IEEE Transactions on Antennas and Propagation*, Vol. 65, No. 2, 903–908, Feb. 2017.

[9] He, J., A. Wu, Z. Fang, Z. Zhang, P. Zhang, W. Wang, and Z. Wang, "A high out-of-band suppression and selective filtering patch antenna," *IEEE Antennas and Wireless Propagation Letters*, Vol. 24, No. 9, 3159–3163, Sep. 2025.

[10] He, Q.-Q., P. Zhou, D. Li, M.-C. Tang, Z. Wu, D. Yi, and M. Li, "A compact, uniplanar, wideband, differential-fed transparent filtenna," *IEEE Antennas and Wireless Propagation Letters*, Vol. 21, No. 4, 735–739, Apr. 2022.

[11] Chen, X., L. Zhu, and M. Li, "Design of wideband, compact, filtering slot antennas enabled by mixed electric/magnetic couplings," *IEEE Transactions on Antennas and Propagation*, Vol. 72, No. 4, 3718–3723, Apr. 2024.

[12] Liu, Q. and L. Zhu, "A compact wideband filtering antenna on slots-loaded square patch radiator under triple resonant modes," *IEEE Transactions on Antennas and Propagation*, Vol. 70, No. 10, 9882–9887, Oct. 2022.

[13] Yin, J.-Y., T.-L. Bai, J.-Y. Deng, J. Ren, D. Sun, Y. Zhang, and L.-X. Guo, "Wideband single-layer substrate integrated waveguide filtering antenna with u-shaped slots," *IEEE Antennas and Wireless Propagation Letters*, Vol. 20, No. 9, 1726–1730, Sep. 2021.

[14] Chen, B.-J., X.-S. Yang, and B.-Z. Wang, "A compact high-selectivity wideband filtering antenna with multipath coupling structure," *IEEE Antennas and Wireless Propagation Letters*, Vol. 21, No. 8, 1654–1658, Aug. 2022.

[15] Cheng, G., J. Zhou, B. Huang, L. Yang, and Z. Huang, "Compact low-profile wideband filtering antenna without additional filtering structure," *IEEE Antennas and Wireless Propagation Letters*,

Vol. 22, No. 10, 2477–2481, Oct. 2023.

[16] Li, L., H. D. Xiong, W. Y. Wu, A. B. Fu, and J. Y. Han, "A t-shaped strips loaded wideband filtering patch antenna with high selectivity," *IEEE Antennas and Wireless Propagation Letters*, Vol. 23, No. 1, 89–93, Jan. 2024.

[17] Zhang, X. Y., W. Duan, and Y.-M. Pan, "High-gain filtering patch antenna without extra circuit," *IEEE Transactions on Antennas and Propagation*, Vol. 63, No. 12, 5883–5888, Dec. 2015.

[18] Liang, G.-Z., F.-C. Chen, H. Yuan, K.-R. Xiang, and Q.-X. Chu, "A high selectivity and high efficiency filtering antenna with controllable radiation nulls based on stacked patches," *IEEE Transactions on Antennas and Propagation*, Vol. 70, No. 1, 708–713, Jan. 2022.

[19] Yang, D., H. Zhai, C. Guo, and H. Li, "A compact single-layer wideband microstrip antenna with filtering performance," *IEEE Antennas and Wireless Propagation Letters*, Vol. 19, No. 5, 801–805, May 2020.

[20] Chen, X., Q. Zhuge, G. Han, R. Ma, J. Su, and W. Zhang, "A wideband harmonic suppression filtering antenna with multiple radiation nulls," *Progress In Electromagnetics Research Letters*, Vol. 112, 17–25, 2023.

[21] Yuan, H., F.-C. Chen, and Q.-X. Chu, "A wideband and high gain dual-polarized filtering antenna based on multiple patches," *IEEE Transactions on Antennas and Propagation*, Vol. 70, No. 10, 9843–9848, Oct. 2022.

[22] Cheng, G., B. Huang, Z. Huang, and L. Yang, "A high-gain circularly polarized filtering stacked patch antenna," *IEEE Antennas and Wireless Propagation Letters*, Vol. 22, No. 5, 995–999, May 2023.

[23] Wang, L., H. Lin, and C. Li, "Miniaturized wideband filtering antenna without additional filtering structures," *Progress In Electromagnetics Research C*, Vol. 163, 222–230, 2026.